A focusing crystal analyser for the rejection of inelastic X-ray scattering

M. A. Hamilton, T. H. Metzger,* A. Mazuelas and T. Buslaps

European Synchrotron Radiation Facility, BP 220, 38043 Grenoble CEDEX, France. E-mail: metzger@esrf.fr

A focusing crystal analyser has been constructed that allows the rejection of inelastic X-ray scattering during diffuse scattering measurements close to an absorption edge. A Johann geometry was obtained by cylindrical bending of perfect silicon and germanium crystals. The choice of reflection, the effect of bending and the contribution of the source size are discussed in relation to the energy resolution. Measurements at the As *K*-edge (11.867 keV) and at the Cs *K*-edge (35.985 keV) are presented to demonstrate that the focusing analyser can be used over a wide energy range. A direct comparison with a flat perfect crystal with comparable energy resolution shows a gain in intensity by a factor of 50.

Keywords: analysers; inelastic X-ray scattering; focusing; bent crystals; energy resolution.

1. Introduction

The use of the resonant (anomalous) part of the X-ray form factor, $f'(E)$, in diffraction measurements allows the scattering power of a particular element to be varied significantly by making small changes to the incident energy. For samples that contain more than one element this variability allows the scattering from a particular element to be enhanced with respect to the other elements in the system. In the case of diffuse scattering it is possible to obtain a difference in the structure factor that contains only the pair correlation functions due to the element of interest by subtracting two measurements at different energies (Buchanan *et al.*, 2001; Ramos *et al.*, 2001). The use of an incident energy close to an absorption edge makes it possible to vary $f'(E)$ but also increases the intensity of inelastic scattering. The main inelastic contributions are Compton scattering and fluorescence or resonant Raman scattering (RRS) (Manninen *et al.*, 1986). During a typical experiment the incident X-ray energy is tuned to a value close to but below the absorption edge and to a value further below the edge, in order to give the maximum contrast in $f'(E)$. The position and intensity of the Compton scattering vary strongly with the scattering angle, 2θ, but do not change rapidly as a function of incident energy. In contrast, the intensity of the fluorescence or RRS varies as $1/(E_{\rm edge}^2 - E_{\rm incident}^2)$ (Fig. 1). The difference in the RRS cross section for the two energies used in the experiment is therefore large. In order to obtain accurate intensity measurements the inelastic scattering must be removed, particularly in the case of diffuse scattering, where the elastic scattering is relatively weak. An experimental solution requires either a detector with sufficient energy resolution or a crystal analyser. The energy resolution that is required can be estimated from the difference between the edge energy and the energies of the $K\alpha$ and $K\beta$ emission lines of, for example, Cs (Table 1).

Typically, a solid-state detector gives an energy resolution that is sufficient to separate the $K\alpha$ contributions but that is not able to remove all of the $K\beta$ contributions (Kappen *et al.*, 2002). Since solid-state detectors with better resolution are not available, only the use of a crystal spectrometer gives the required resolution. Flat analyser crystals are commonly used for this purpose and are suitable for applications in crystallography where high angular resolution is required. However, in the case of diffuse scattering, the angular resolution can be relaxed and a spectrometer that accepts a larger divergence is desirable. This setup can be achieved by a focusing geometry based either on a mosaic crystal (Ice & Sparks, 1990) or on a bent perfect crystal. In this paper the design and use of a focusing analyser based on a bent perfect crystal is described. This analyser allows an energy resolution that is an order of magnitude better than that of a typical solid-state detector while giving a gain in intensity of a factor 50 compared with a system based on a flat perfect crystal.

2. Description of the focusing analyser

The focusing conditions for such an analyser are described by the Rowland circle (as shown in Fig. 2), and in order to obtain this geometry it is necessary to grind the crystal to make a Johansson monochromator. In this case each point on the crystal sees the point-like source under the same Bragg angle. A crystal that is simply bent to the required bending radius introduces some error and is called a Johann monochromator (Suortti *et al.*, 1986). The useful energy range for anomalous-scattering experiments is large, and therefore the simpler Johann system was chosen so that the system would be widely applicable. The bending radius of the crystal (ρ) is given by,

$$\rho = x / \cos(\chi - \theta_{\rm B}), \qquad (1)$$

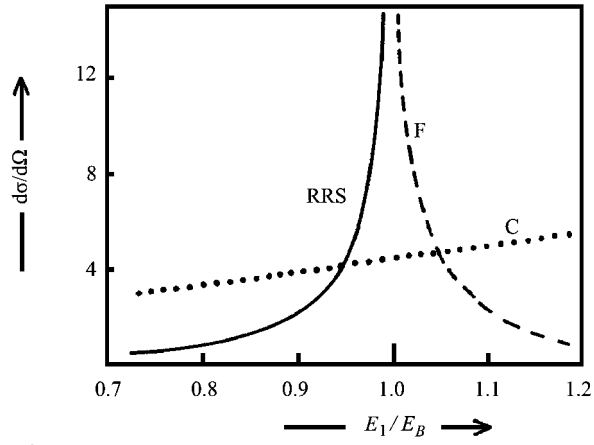

Figure 1
Relative cross section for Compton scattering (C), fluorescence (F) and resonant Raman scattering (RRS) at incident energies around the absorption edge ($E_{\rm B}$). [Reproduced from the *International Tables for X-ray Crystallography* (1995).]

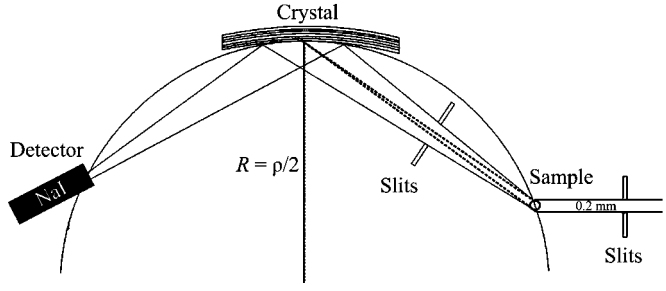

Figure 2
Rowland circle for a symmetrically cut crystal in a Johann geometry. The dashed line shows the divergence at the crystal due to the source size.

Table 1
The emission lines of RRS contributions at the Cs *K*-edge (36 keV).

Data from the *International Tables for X-ray Crystallography* (Wilson, 1995).

Transition	Emission line	Energy (keV)	Shift from elastic energy (keV)
K–*L*II	$K\alpha 2$	30.625	5.357
K–*L*III	$K\alpha 1$	30.973	5.009
K–*M*II	$K\beta 3$	34.919	1.062
K–*M*III	$K\beta 1$	34.987	0.995
K–*N*II	$K\beta 2$	35.822	0.160

where x is the distance from the sample (source) to the analyser, θ_B is the Bragg angle and χ is the miscut of the crystal. In the symmetric case the sample–analyser and analyser–detector distances are equal, with zero miscut ($\chi = 90^\circ$). For a fixed sample–analyser distance, the bending radius depends on the incident energy, the d-spacing of the crystal and the reflection that is used. The Bragg angle also affects the energy resolution *via* the derivative of Bragg's law,

$$\Delta E/E = \Delta\theta \cot(\theta_B), \tag{2}$$

where $\Delta\theta = \Delta\theta_{crystal} + \Delta\theta_{source}$.

Therefore, for a given energy, the type of crystal and reflection determines the bending radius and energy resolution. The sample–analyser distance was fixed at 0.5 m, and a range of crystal reflections were considered in order to estimate the required bending radius *via* (1). At the same time, the energy resolution for each solution was calculated given that the two principal contributions to $\Delta\theta$ in (2) are the width of the reflectivity curve of the crystal and the source size. To make this calculation possible the reflectivity curves for a range of crystals, reflections and bending radii were simulated using the *XOP* software (Sanchez del Rio & Dejus, 1997).† These curves (Figs. 3 and 4) show the diffracted intensity as a function of incident angle (with respect to the Bragg angle at zero).

The shape of the reflectivity curves is determined by absorption and, in the case of Fig. 3, by the amount of bending. The greater the bending the broader the diffraction curve and the worse the resolution. The limit of bending and the resultant distortion of the crystal are also affected by the material and its thickness. A 1 mm-thick crystal was chosen in order to allow a bending radius of less than 3 m while maintaining an acceptable level of distortion and a reasonable efficiency at an energy of up to 36 keV. The dependence of the reflectivity curve on different crystal reflections is shown in Fig. 4. As the order of reflection is increased, the integrated reflectivity reduces for a limited change in the resolution. So the use of a higher-order reflection is not favourable with respect to the intensity.

The source size also has an effect on the energy resolution, since the source size defines a $\Delta\theta$ at the analyser crystal that is given by the size divided by the sample–analyser distance (this divergence is shown in Fig. 2 by the dashed lines). As the energy resolution also depends on the Bragg angle, a higher-order reflection gives a smaller contribution and so an improved resolution. A summary of the calculations for the bending radius and resolution for various crystals is given in Table 2.

For a given energy and source size, the energy resolution improves as the order of reflection is increased. Because of the effect of absorption on the width of the diffraction curve, Ge crystals have a smaller crystal contribution. In both cases improved resolution is only gained at the expense of the integrated reflectivity of the crystal. To implement these ideas, a bending device has been constructed for use

† *XOP* is available from the ESRF website at http://www.esrf.fr/computing/scientific/xop/.

Table 2
A calculation of the bending radius and energy resolution for a range of crystal reflections at an energy of 36 keV.

The source size is taken to be 0.2 mm at 0.5 m from the analyser. The crystal contributions are from *XOP* simulations. (The two contributions are added in quadrature.)

	Si(111)	Si(400)	Si(422)	Ge(111)	Ge(400)
θ_B (°)	3.20	7.41	9.15	3.07	7.11
ρ (m)	8.96	3.88	3.14	9.34	4.04
ΔE_{source} (eV)	250	108	87	261	112
$\Delta E_{crystal}$ (eV)	156	153	141	31	11
ΔE_{Total}	295	187	150	263	112

with a range of crystal reflections (Table 2). In order to achieve cylindrical bending, a 1 mm-thick crystal of length 80 mm and width 60 mm was held at one end by a support with a steel lever clamped at the other (Fig. 5). This lever is pushed by a pin that is mounted on a motorized stage to allow the remote control of the bending force. The vertical position of the pin can be adjusted by a second stage to minimize the twist that is induced in the crystal by the bending force. This simple system is sufficient to allow cylindrical bending to radii of

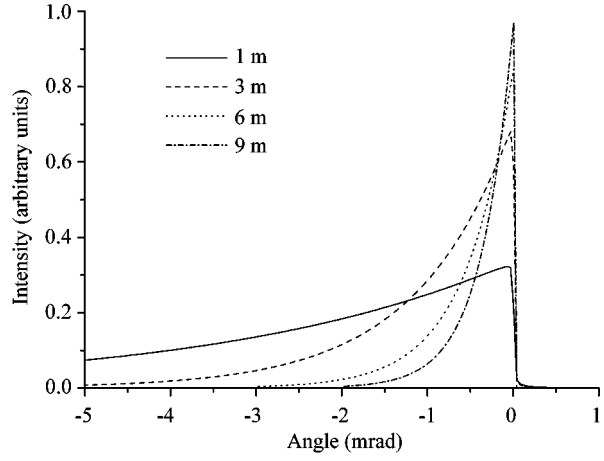

Figure 3
Reflectivity curve of a 1 mm-thick Si(111) crystal for various bending radii at 36 keV (*XOP* software).

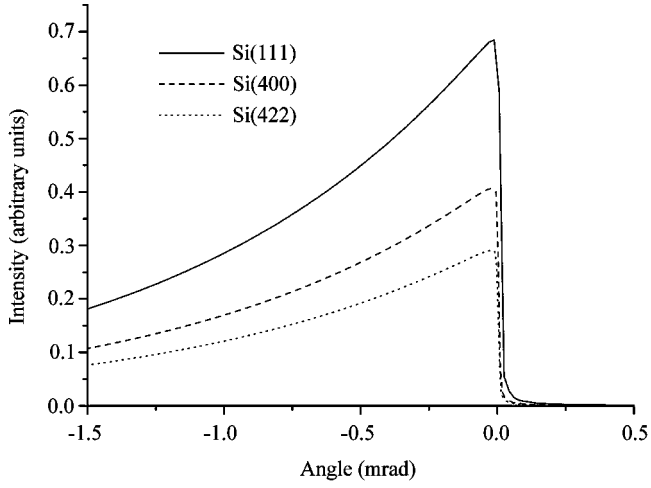

Figure 4
Reflectivity curve for various reflections of Si for a bending radius of 3 m at an energy of 36 keV (*XOP* software).

less than 3 m. This design was adapted from the high-resolution Compton spectrometer that is operating at the ESRF beamline ID15B (Suortti *et al.*, 1999).

3. Experimental results

The measurements were carried out at beamline ID1 of the ESRF. This is an undulator beamline that has been designed for anomalous-scattering measurements. The monochromator consists of an Si(111) or (311) pair, which gives a continuous energy range of 2–42 keV. A pair of curvable Si mirrors on either side of the monochromator allow harmonic rejection and vertical focusing. The analyser is mounted on the detector arm of the diffractometer, which has additional rotation circles (for the analyser and detector, as shown in Fig. 2). Note that the analyser operates in the vertical scattering plane. The bending device is attached to a tilt stage and a linear translation table, which allow the crystal to be quickly and accurately aligned in the beam. An NaI(Tl) scintillation detector was used for all of these measurements. The following procedure was used to align the crystal with the Rowland circle. The bending device was set to the required bending radius by observing the focusing of a laser spot. As the bending force is motorized, this parameter could then be refined on the diffractometer by measuring fluorescence lines at an energy close to that to be used for the measurements. The bending radius was assumed to be correct when the intensity of the lines was a maximum and the width a minimum (and close to the calculated value). In order to demonstrate the use of the analyser at more than one energy, initial tests were carried out at the As *K*-edge (11.867 keV), with later measurements at the Cs *K*-edge (35.985 keV). The actual contributions of the source size and the bending quality of an Si(111) crystal were tested by measurements of the fluorescence from As in a sample of GaAs at an incident energy of 150 eV above the *K*-edge of As. The width and shape of the $K\alpha$ fluorescence lines demonstrate the energy resolution and bending quality of the analyser. The source size was varied by changing the vertical size of the incident beam, *via* the final beam-defining slit before the sample, over a range of 0.1–0.3 mm.

Note that for reflection geometry the illuminated area of the sample as seen by the analyser, and therefore also the energy resolution, varies with 2θ. The measurements were therefore carried out at a fixed scattering angle. The effect of the source profile on the resolution is described by Ice & Sparks (1990). Furthermore, given that the resolution has more than one contribution, it was confirmed by simulation that the crystal contribution was smaller than the effect of the source size. The results show a clear broadening of the fluorescence lines as the vertical beam size is increased (Fig. 6), which proves that the resolution becomes worse with increasing source size (given that this is the largest single contribution to the resolution function). In addition, because of various errors (bending error, anticlastic twist and Johann error), the crystal does not fit the Rowland circle exactly, and thereby small angular aberrations are introduced that will reduce the energy resolution (Suortti *et al.*, 1986). It was possible to vary the area of the bent crystal that was used, by changing the size of the slit between the sample and analyser. The size along the bending direction was varied between 1 and 5 mm. For the smallest slit size, only the centre of the crystal was illuminated, and in this region the deviation from the Rowland circle is the smallest. Indeed, the width of the fluorescence lines that were measured confirm that the resolution becomes significantly worse as the edges of the crystal are included (Fig. 7).

In order to determine the gain in intensity that can be achieved with a focusing geometry as compared with a flat crystal, the same fluorescence lines were measured with both systems. Care was taken to make the measurements directly comparable by using an identical setup in each case. However, an additional slit at the detector position was required in the non-focusing case, as the Bragg angle between the beam and the crystal changes along the axis of diffraction. The energy resolution is therefore improved only by reducing the length of the crystal that the detector 'sees' at the expense of the intensity. With a bent crystal this is not the case, and aside from errors in obtaining a perfect focusing geometry, as already discussed, only one Bragg angle is accepted by the system. The size of the detector slit was chosen to

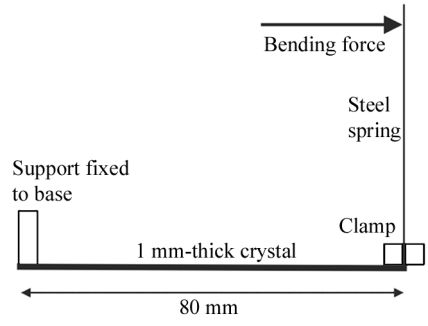

(*a*)

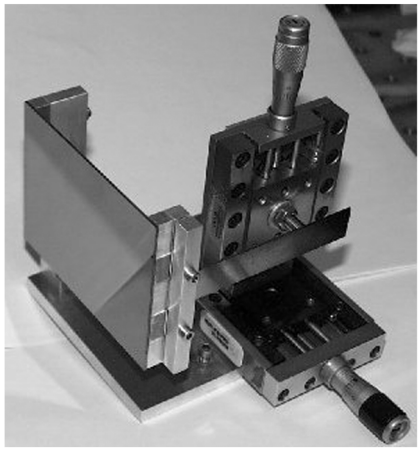

(*b*)

Figure 5
(*a*) Schematic view that shows the principle of operation of the bender and (*b*) the bending device with translation stages.

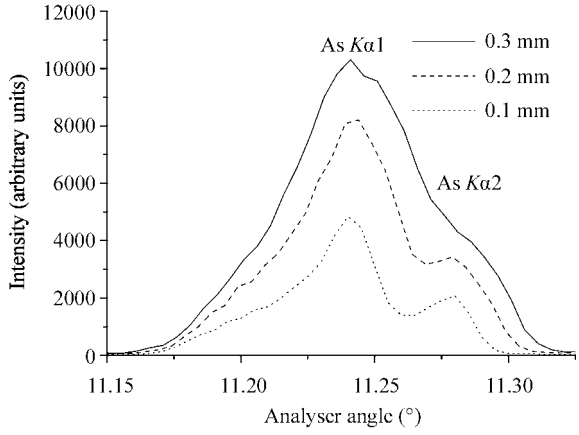

Figure 6
Effect of source size on the $K\alpha$ fluorescence lines of As. The source size was varied *via* the vertical gap of the beam-defining slit (to 0.3, 0.2 and 0.1 mm).

match the energy resolution of the focusing system. Fig. 8 demonstrates that for a similar energy resolution the gain in intensity is a factor of 50.

The focusing geometry has been applied in several anomalous X-ray diffraction (AXD) experiments. These include measurements of molten salts, aqueous solutions and amorphous thin films at the In (28 keV), I (33 keV) and Cs (36 keV) *K*-edges. In each case the Si(422) reflection was used to reduce the source-size contribution to the resolution while maximizing the efficiency of the analyser system. The expected energy resolution according to Table 2 is 150 eV. Fig. 9 shows a θ–2θ scan of the analyser for a molten CsCl sample at an incident energy of 10 eV below the Cs *K*-edge. The peak at the highest energy is the elastic peak. Note that for diffuse scattering at this angle and with an incident energy very close to the edge the RRS intensity is *more* intense than the elastic scattering. The shoulder on the elastic line is the *K*–*N*II RRS contribution, which is shifted from the incident energy by 160 eV. The measured resolution therefore agrees with the calculated value. The most intense peak is the *K*–*M*II,III RRS, which is shifted by 1062 and 995 eV; the two peaks are not resolved. Underlying this peak is a weaker and broader feature that arises from the Compton scattering; this feature is also shifted by little more than 1 keV at this scattering angle ($2\theta = 60^\circ$). It is clear from Fig. 9 that the *K*–*N* RRS emission line and the tail of the Compton distribution are not fully resolved and so contribute to the measured intensity. Indeed, the *K*–*N* line introduces a significant error in the measured intensity at this angle (∼30%), which is not acceptable. It is suggested that an energy scan such as this can be made at each point in the *Q*-range and the remaining *K*–*N* contribution removed in the subsequent analysis. Although time-consuming, this procedure is made practical by the tremendous increase in count rate that is obtained. In principle it is possible to achieve the same result more directly by improving the energy resolution of the analyser system, the main contribution to the energy resolution being the beam divergence at the analyser crystal due to the source size and distance. A smaller vertical beam size and/or an increased sample–analyser distance would therefore be effective ways of improving the performance. This was not possible at beamline ID1 because of the optics (a minimum beam height at the sample of 0.2 mm) and the fixed sample–analyser distance (defined by the diffractometer). Furthermore, because of the dominance of the source-size contribution, the use of a more sophisticated bending system or crystal design is not considered advantageous.

4. Conclusions

A focusing analyser system based on a bent Si crystal has been described, which allows inelastic scattering components to be rejected during measurements close to an element's absorption edge. The bending device and alignment of the spectrometer are relatively straightforward, and the improvement in efficiency is a factor of 50, more than an order of magnitude. A simple technique to refine the bending radius is proposed, and the effect of deviations of the crystal from the Rowland circle near the edges has been measured. The effect of the source size on the resolution has also been demonstrated. The measurements of resolution for a range of incident energy and crystal reflections agree well with calculations. This system has been used for anomalous-scattering measurements of amorphous thin films, molten salts and aqueous solutions.

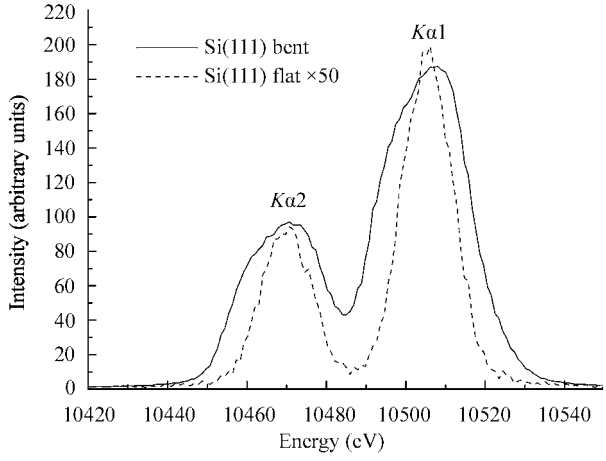

Figure 8
As *Kα* fluorescence with a flat Si(111) crystal and a cylindrically bent crystal in the Rowland circle geometry. The width of the lines is comparable in each case, and the average gives a resolution of 20 eV.

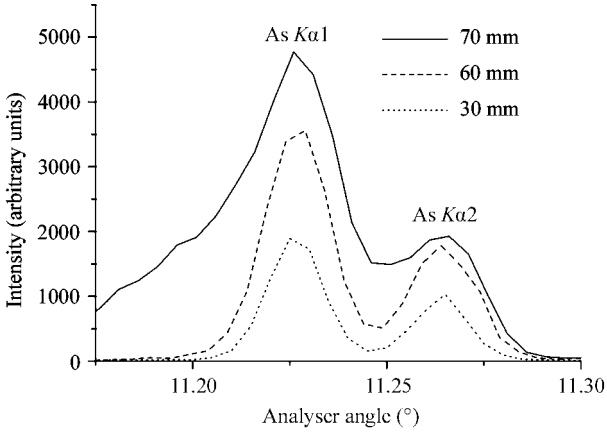

Figure 7
Resolution as a function of illuminated crystal length (with As *Kα* fluorescence). The crystal is 80 mm long. The resolution decreases as a larger area of the crystal is used because of deviations from the Rowland circle (bending error *etc.*).

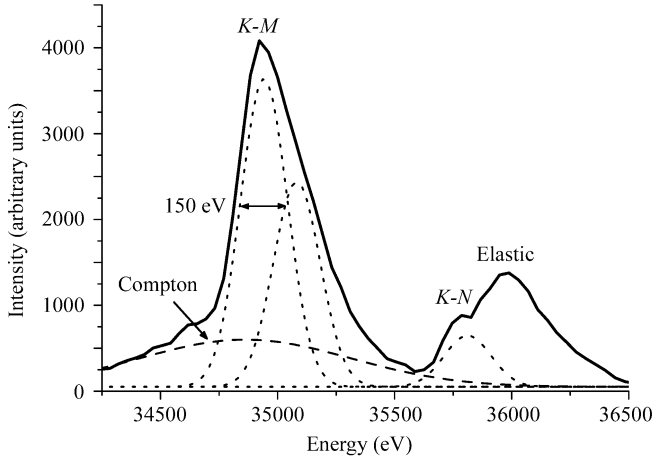

Figure 9
Results collected with the bent Si(422) crystal at the Cs *K*-edge showing RRS (*K*–*M*, *K*–*N*) and Compton scattering. The Gaussian curves are a schematic representation of the RRS (dots) and Compton (dash) contributions.

We would like to thank the optics group of the ESRF for the supply of Si and Ge crystals and Adrian Barnes for the data collected at the Cs *K*-edge.

References

Buchanan, P., Barnes, A. C., Whittle, K. R., Hamilton, M. A., Fitch, A. N. & Fischer, H. E. (2001). *Mol. Phys.* **99**, 767–772.
Ice, G. E. & Sparks, C. J. (1990). *Nucl. Instrum. Methods Phys. Res. A*, **291**, 110–116.
Kappen, P., Troger, L., Materlik, G., Reckleben, C., Hansen, K., Grunwaldt, J.-D. & Clausen, B. S. (2002). *J. Synchrotron Rad.* **9**, 246–253.
Manninen, S., Suortti, P., Cooper, M. J., Chomilier, J. & Loupias, G. (1986). *Phys. Rev. B*, **34**, 8351–8356.
Ramos, S., Neilson, G. W., Barnes, A. C. & Mazuelas, A. (2001). *J. Phys. Chem.* B**105**, 2694–2698.
Sanchez del Rio, M. & Dejus, R. J. (1997). *Proc. SPIE*, **3152**, 148–157.
Suortti, P., Buslaps, T., Fajardo, P., Honkimaki, V., Kretzschmer, M., Lienert, U., McCarthy, J. E., Renier, M., Shukla, A., Tschentscher, Th. & Meinander, T. (1999). *J. Synchrotron Rad.* **6**, 69–80.
Suortti, P., Pattison, P. & Weyrich, W. (1986). *J. Appl. Cryst.* **19**, 336–342.
Wilson, A. J. C. (1995). *International Tables for Crystallography*. Dordrecht: Kluwer.

 Received 9 August 2002 • Accepted 27 December 2002